Generation of high-energy localized vibrational modes in nonlinear Klein-Gordon lattices

Ole Bang[1,2] and Michel Peyrard[1]

[1] *Laboratoire de Physique, Ecole Normale Supérieure de Lyon, 46 Allée d'Italie, 69364 Lyon Cédex 07, France*

[2] *Optical Sciences Centre, The Australian National University, Canberra Australian Capital Territory 0200, Australia*

(Received 7 July 1995; revised manuscript received 3 November 1995)

We study numerically the exchange of energy and momentum between colliding breathers in nonlinear Klein-Gordon lattices as a means of obtaining localization of energy. Statistical calculations show a clear preference of the larger breather to take energy from the smaller one in the whole energy range of interest. Thus it represents an effective mechanism for energy localization in nonlinear Klein-Gordon lattices, originating from the discreteness and nonintegrability of the system. To get initial conditions for our simulations we numerically calculate exact single-frequency static breather solutions using a technique recently discovered by Flach [Phys. Rev. E **51**, 3579 (1995)].

PACS number(s): 03.40.Kf, 63.20.Pw, 46.10.+z

I. INTRODUCTION

In many physical systems spins or atoms may be considered as harmonically coupled to nearest neighbors only, and subjected to a nonlinear external potential. In this case the Hamiltonian of the system can be written as

$$H = \sum_n \left[\frac{1}{2}\dot{U}_n^2 + \frac{1}{2}(U_n - U_{n-1})^2 + V(U_n) \right] , \tag{1}$$

$$V'(0) = 0 , \quad V''(0) = \omega_d^2 > 0 ,$$

where $U_n(t)$ is the on-site degree of freedom (e.g., interatomic distance) and $V(U_n)$ is an external potential, representing the combined influence of the surrounding crystal or macromolecule and external effects, such as an electric or magnetic field. The parameter ω_d is the minimum frequency of the harmonic (optical) vibrations of the chain. The equation of motion for such a system is the discrete nonlinear Klein-Gordon (KG) equation

$$\ddot{U}_n - (U_{n+1} - 2U_n + U_{n-1}) + V'(U_n) = 0 . \tag{2}$$

This discrete set of ordinary differential equations has have been widely used in the study of physical phenomena such as dislocations [1], ferroelectric domain walls [2], ferromagnetic domain walls [3], DNA dynamics [4], and Josephson junctions [5].

Depending on the shape of the on-site potential $V(U_n)$, a nonlinear lattice with the Hamiltonian (1) may sustain several types of nonlinear excitations. If $V(U_n)$ has multiple degenerate minima, as, for instance, in the Frenkel-Kontorova model, for which $V(U_n)$ is a sinusoidal function, topological excitations with a kink shape interpolating between adjacent minima can exist. Moreover, even when $V(U_n)$ has only a single absolute minimum, localized vibrational modes, sometimes called discrete breathers, can exist. These local modes have been the subject of intense research in the last few years since the work of Sievers and Takeno [6], following an earlier prediction of their existence in a narrower context by Kosevich and Kovalev [7]. This interest is motivated by the interesting properties of discrete breathers: They are nontopological excitations without an energy threshold for their creation; they exist in a large variety of nonlinear lattices, whether nonlinearity arises from the interaction [8–10] or from an on-site potential as in (1) [11–19]; their existence is associated with a localization of energy.

While physicists are familiar with disorder-induced localization, it may seem surprising that energy can stay localized in a translationally invariant system. This is an effect of nonlinearity that is not trivial because it also requires the *discreteness* of the lattice. Except in the specific case of the integrable sine-Gordon model [20, 21], stable breathers do not exist in systems described by a partial differential equation that is a continuous version of Eq. (2), with the second difference replaced by a second derivative. This has been proved for, e.g., the continuous Φ^4 model [22]. Mackay and Aubry [19] have shown that, on the contrary, if discreteness effects are sufficient, breathers are exact solutions for a nonlinear lattice, i.e., they are rigorously stable. Although this work has shown mathematically the possible *existence* of stable nontopological local modes in a homogeneous lattice, confirming numerous analytical and numerical investigations of approximate solutions [11–18], the question of their *creation* is still open. Local modes can only be physically relevant if there is an efficient mechanism that can lead to their formation. We show in this paper that such a mechanism of self-localization of energy in a homogeneous lattice described by Hamiltonian (1) does exist, and that discreteness is not only necessary to stabilize the breathers, as shown by Mackay and Aubry, it also provides the pathway to their formation.

The first step toward nonlinear energy localization can be achieved through Benjamin-Feir instability [23], i.e., the spontaneous modulation of a large amplitude plane wave, which tends to split into wave packets. Modulational instability exists in a lattice as well as in a continuum medium, although discreteness may drastically

change the conditions for instability [24, 25]. However, the maximum energy of breathers created by this process is bounded because each breather collects the energy of the initial plane wave over the modulational length λ, so that its energy cannot exceed $E_{\max} = \lambda\epsilon$, where ϵ is the energy density of the wave. One possible way of creating breathers with energies exceeding $E_{\max}$ would be if one breather could collect the energy from several others. It is evident that there will be an energy exchange, as well as radiation of phonons, when two discrete breathers collide, due to the nonintegrability of the nonlinear KG lattice, Eq. (2). The question is whether the exchange occurs at random, such that on average there is no transfer of energy, or whether there is a preference for, e.g., the larger one to take energy from the smaller one. This question was examined numerically by Dauxois and Peyrard [12] and indeed a clear tendency for collisions to favor the growth of the larger breather was observed. However, a definite conclusion cannot be made from a few experiments because the energy exchange depends on the relative phase and energy of the breathers. It is the aim of this paper to statistically consider all possible values of the relative phase and energy during collisions, in order to check if a preference really exists. Moreover, we want also to determine whether there are conditions on the symmetry of the potential $V(U_n)$ to observe localization.

The paper is organized as follows: First we present the specific model and formulate the numerical problem we would like to consider: a low energy moving breather colliding with a high energy static breather. In order to make accurate measurements, the initial condition must be selected carefully. The low energy moving breather is taken as a third order semidiscrete solution, derived in an earlier work [26], while the high energy breather is studied in more detail. We use a mapping technique recently discovered by Flach [16] to derive numerically exact single-frequency static breather solutions. The frequency domain, in which such solutions exists, is also identified. Finally we present and discuss the statistical numerical calculations of the energy and momentum transfer during collision.

II. THE MODEL AND THE FORMULATION OF THE PROBLEM

We consider a particular physical system described by the Hamiltonian (1), a chain of equally spaced particles of unit mass coupled harmonically to their nearest neighbors with unit elastic coefficient and subjected to the on-site substrate potential

$$V(U_n) = \omega_d^2(\tfrac{1}{2}U_n^2 - \alpha\tfrac{1}{3}U_n^3 - \beta\tfrac{1}{4}U_n^4), \quad U_n \leq 1 . \quad (3)$$

Here U_n is the displacement of the particle at site n from its equilibrium position, and ω_d, α, and β are real parameters. For $\beta = 0$, V becomes the nonsymmetric Φ^3 potential, which, e.g., has been used in the study of DNA, since it resembles the Morse potential for $U_n \leq 1$ [11]. For $\alpha = 0$, V becomes the symmetric Φ^4 potential, e.g., used in the modeling of ferroelectric domain walls [2]. In general V can be viewed as a medium amplitude expansion of any potential around a minimum.

The Hamiltonian energy of the chain is

$$H = \sum_n \mathcal{H}_n = \sum_n \Big[\tfrac{1}{2}\dot{U}_n^2 + \tfrac{1}{2}(U_n - U_{n-1})^2 + \omega_d^2(\tfrac{1}{2}U_n^2 - \alpha\tfrac{1}{3}U_n^3 - \beta\tfrac{1}{4}U_n^4)\Big] , \quad (4)$$

where $\mathcal{H}_n$ is the Hamiltonian energy density. It gives the equations of motion

$$\ddot{U}_n - (U_{n+1} - 2U_n + U_{n-1}) + \omega_d^2(U_n - \alpha U_n^2 - \beta U_n^3) = 0 . \quad (5)$$

The linearized equation ($\alpha = \beta = 0$) has plane-wave solutions, for which the frequency ω and the wave number q satisfy the dispersion relation

$$\omega^2 = \omega_d^2 + 4\sin^2(\tfrac{1}{2}q) . \quad (6)$$

The phonon band has an optical shape and is shown in Fig. 1(a). The minimum phonon frequency, ω_d, is a measure of the strength of the on-site potential, which controls the discreteness. In this paper we are interested in the case where discreteness dominates, i.e., $\omega_d^2 \gg 1$. We have chosen $\omega_d^2 = 10$.

As indicated in the Introduction, our aim is to study how collisions can lead to the formation of discrete breathers with an energy beyond the maximum energy $E_{\max}$ that can be achieved by modulational instability. In addition we want to characterize the large amplitude nonlinear excitations created in the process, and in particular discuss their stability. This goal determines the first steps of the work because we must first set up appropriate initial conditions for the collisions and also define criteria for stability of the discrete breathers.

We simulate collisions between small amplitude moving breathers and large amplitude static ones, and measure the change in energy and momentum of the larger breather. The smaller breather is supposed to be excited by modulational instability. The larger breather is also assumed to have been excited by modulational instability, but we further assume that it has already increased its energy through, e.g., collisions with other breathers. The initial condition for a simulation is depicted in Fig. 2, defining also the breather parameters. Subscript 0 always refers to the small breather, while 1

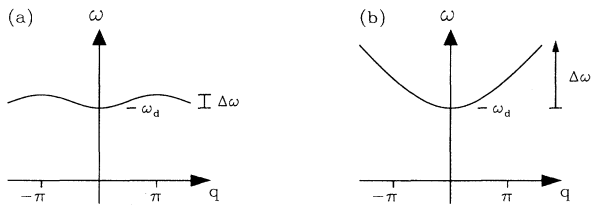

FIG. 1. (a) Phonon dispersion relation, $\omega^2 = \omega_d^2 + 4\sin^2(q/2)$, for Eq. (5). The bandwidth $\Delta\omega$ is finite. (b) Phonon dispersion relation, $\omega^2 = \omega_d^2 + q^2$, for the continuum approximation of Eq. (5). Here the bandwidth is infinite. $\omega_d^2 = 10$.

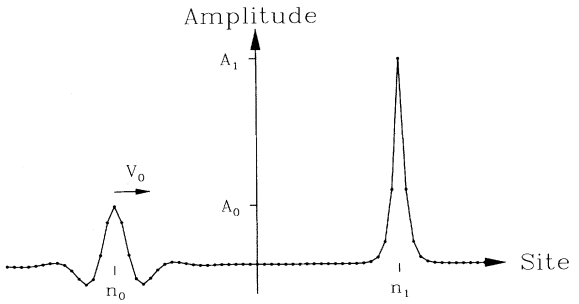

FIG. 2. Parameter definition and setup for the simulation of a collision between a small amplitude breather moving towards a large amplitude static breather.

refers to the large one. Since we want to characterize the energy exchange mechanism by a detailed study of individual collisions, we must perform accurate measurements. This is only possible if the breathers that collide are good solutions with well defined parameters. In the derivation of these solutions for a lattice, which does not have a continuous translational-invariance symmetry, we must consider separately the case of moving and static breathers.

The nonlinear KG lattice, Eq. (5), has never been solved exactly analytically. The best currently known small amplitude moving breather solution is a third order semidiscrete solution [26]. This solution is completely defined by three parameters, the amplitude A_0, the envelope velocity V_0, and an internal wave number q_0, which all have upper limits for the solution to be classified as good, i.e., to move with no significant radiation of energy with a measured velocity and amplitude close to the predicted values. As the amplitude is increased, the width of the breather decreases and it feels the lattice discreteness more and more and can even become completely pinned to a single site. Although it is more complicated for breathers that have an internal degree of freedom [14] than for kinks [27], this trapping effect has the same fundamental origin in both cases, the breaking of the continuous translational invariance, which introduces an effective lattice potential in which the excitation moves. From dislocation theory this potential is known as the Peierls-Nabarro (PN) potential [28].

Numerically the maximum amplitude, above which breathers are completely pinned by the discreteness of the lattice, was found to $A_0^{\max} = 0.4$ for $\omega_d^2 = 10$, and the maximum linear group velocity

$$V_g^{\max} = V_g(q = q_0^{\max}) = \sin(q_0^{\max})/\sqrt{\omega_d^2 + 4\sin^2(q_0^{\max}/2)} \quad (7)$$

was found to represent the upper limit of the velocity of breathers in the system given by Eq. (5) [26]. Here the maximum wave number is defined as

$$\cos(q_0^{\max}) = 1 + \tfrac{1}{2}\omega_d^2(1 - \sqrt{1 + 4/\omega_d^2}) \ . \quad (8)$$

For $\omega_d^2 = 10$ the maximum wave number is $q_0^{\max} = 1.49$, resulting in a limiting velocity of $V_0^{\max} = 0.29$. In our statistical calculations we fix the wave number at $q_0 = 0.2$ and consider velocities around $V_0 = 0.2$, and amplitudes around $A_0 = 0.1$ and 0.2. This assures that the solution is good, and thus that the time of collision can be predicted. For the explicit expression of the third order semidiscrete solution we refer to Ref. [26].

Because of the low amplitude of the small breather a semidiscrete multiple-scale perturbation expansion can be applied to find good solutions, using the amplitude as the small parameter. For the larger breather we consider amplitudes in the range between 0.34 and 0.86, which in general is above the limit for pinning. In this range one has to take the full discreteness into account and thus the semidiscrete solution cannot be used. Since we need solutions in this regime for our analysis we devote a section to their numerical derivation.

III. EXACT STATIC SOLUTIONS

There are very few methods available to calculate exact high amplitude discrete solutions for excitations like breathers, which have internal dynamics. Highly localized solitary wave solutions, which can be moving or static, have been found numerically in discrete nonlinear Schrödinger (NLS) type equations using spectral collocation and path-following methods [29, 30]. This is possible because of the special structure of the nonlinearity in this equation, where the frequency terms arise in a linear manner. Although the path-following technique has been applied to many other nonintegrable lattice equations [29, 31] the use of this technique for discrete nonlinear KG lattices, where the frequency terms arise nonlinearly, seems limited and correspondingly attempts to apply it in this case have failed [29]. There is, however, another numerical approach recently discovered by Flach [16] that can be used. To implement it, it is useful to understand the role of discreteness in the stabilization of breathers.

The comparison of the dispersion curves for a lattice [Fig. 1(a)] and its continuum counterpart [Fig. 1(b)] allows a qualitative understanding. A first condition for the existence of local modes is that their frequency lies outside of the phonon band, otherwise the breathers would lose energy by radiating nonlocalized linear plane waves. Since the phonon band of the lattice has a finite width, $\omega_d^2 \le \omega^2 \le \omega_d^2, +4$ while that of the corresponding continuum system has an infinite width, $\omega^2 \ge \omega_d^2$, this condition is obviously easier to satisfy in the discrete case. However, for breathers with a frequency $\omega_1 < \omega_d$ that lies below the phonon band, there are additional stability conditions. Due to the nonlinearity of the equations of motion (5) harmonics $k\omega_1$ of the breather frequency are excited and must also lie outside the phonon band to avoid coupling to linear plane waves. The resulting bands of nonexistence for breathers are (bands of nonexistence)

$$\omega_d^2 \le (k\omega_1)^2 \le \omega_d^2 + 4 \ , \quad k = 1, 2, \ldots \ . \quad (9)$$

In the continuum limit, for which the upper limit of the phonon band extends to $+\infty$, any frequency ω_1 will have

harmonics in the phonon band and breathers cannot exist, unless there are special orthogonality relations between the higher harmonics and the plane waves as in the sine-Gordon case [21]. The necessary condition of existence, that ω_1 must not correspond to one of the forbidden bands defined by Eq. (9), is, however, not sufficient. It was further proven by Flach and co-workers [13] that, provided the solution exists, it will be linearly unstable if its frequency lies in the bands (bands of instability)

$$\omega_d^2 \leq [(n/2)\omega_1]^2 \leq \omega_d^2 + 4 \ , \quad n = 1, 2, \ldots \ . \tag{10}$$

It should be noticed that these existence and stability conditions rule out breathers with two or more internal frequencies. Such multifrequency excitations, which have been observed in numerical simulations, cannot be stable because some combination frequency always will lie in the phonon band. In the present context we will restrict ourselves to single-frequency discrete breathers with a frequency lying in the gap, and fulfilling the relation (band of consideration)

$$(\tfrac{2}{3})^2(\omega_d^2 + 4) \leq \omega_1^2 \leq \omega_d^2 \ . \tag{11}$$

According to Eqs. (9) and (10) such breathers can exist and be stable.

The method discovered by Flach [16] can be used to obtain exact single-frequency static solutions for our high amplitude breather. However, the parameter range in which solutions can be found depends on the form of the potential (Φ^3 or Φ^4). The idea is to start from an expansion of U_n in a Fourier series,

$$U_n(t) = \sum_{k=-\infty}^{\infty} A_{n,k} \exp(ik\omega_1 t) \ , \tag{12}$$

where the Fourier components satisfy the relations

$$A_{n,k} = A_{n,-k} \ , \quad A_{n,k} \to 0 \ \text{ for } \ n, k \to \pm\infty \ , \tag{13}$$

in order for the solution to be real and localized. Inserting the expansion in the equation of motion (5) we get

$$(\omega_d^2 - k^2\omega_1^2)A_{n,k} - (A_{n+1,k} - 2A_{n,k} + A_{n-1,k}) - \omega_d^2 F_{n,k} = 0 \ , \tag{14}$$

where $F_{n,k}$ contains the nonlinear terms. Introducing a finite cutoff frequency, $k_{\max}\omega_1$, $F_{n,k}$ becomes

$$F_{n,k} = \alpha \sum_{p=p_1}^{p_2} (A_{n,p}A_{n,k-p}) + \beta \sum_{p=-k_{\max}}^{k_{\max}} \sum_{q=q_1}^{q_2} (A_{n,p}A_{n,q}A_{n,k-p-q}) \ , \tag{15}$$

where the limits in the sums are given by

$$\begin{aligned} p_1 &= \max(-k_{\max}, k - k_{\max}), \\ q_1 &= \min(-k_{\max}, k - p - k_{\max}), \\ p_2 &= \max(k_{\max}, k + k_{\max}), \\ q_2 &= \min(k_{\max}, k - p + k_{\max}) \ . \end{aligned} \tag{16}$$

The technique is now to reformulate Eq. (14) and write it as a map, which can be used to find solutions by numerical iteration. This is done in two ways:

$$A_{n,k}^{(j+1)} = \frac{1}{k^2\omega_1^2}\left[\omega_d^2 A_{n,k}^{(j)} - (A_{n+1,k}^{(j)} - 2A_{n,k}^{(j)} + A_{n-1,k}^{(j)}) - \omega_d^2 F_{n,k}^{(j)}\right] \quad \text{(map A)}, \tag{17}$$

$$A_{n,k}^{(j+1)} = \frac{1}{\omega_d^2}\left[k^2\omega_1^2 A_{n,k}^{(j)} + (A_{n+1,k}^{(j)} - 2A_{n,k}^{(j)} + A_{n-1,k}^{(j)}) + \omega_d^2 F_{n,k}^{(j)}\right] \quad \text{(map B)}, \tag{18}$$

where the upper label indicates the number of iteration. Without the upper labels Eqs. (17) and (18) are identical, and thus any fix point of map A will also be a fix point of map B, and a solution to the original Eq. (14). An obvious fix point is the zero solution, $A_{n,k} = 0$ for all (n, k). If we linearize around this fix point and assume that the second difference is 0, we obtain the respective eigenvalues

$$\lambda_{n,k}^{\mathrm{A}} = \frac{\omega_d^2}{k^2\omega_1^2} \ , \quad \lambda_{n,k}^{\mathrm{B}} = \frac{k^2\omega_1^2}{\omega_d^2} \ , \tag{19}$$

where the label indicates the corresponding map.

Maps A and B have the important property that for a given pair (n, k) their eigenvalues are positive and inverse to each other, $\lambda_{n,k}^{\mathrm{A}}\lambda_{n,k}^{\mathrm{B}} = 1$. This can be used to construct a new map C, which is composed out of maps A and B in an appropriate way, depending on the particular problem one wants to solve. In our case we want to find symmetric single-frequency breather solutions centered on a lattice site, with frequencies in the band given by Eq. (11). Thus we choose the map with eigenvalue larger than 1 for the main frequency at the center site $(n, k) = (0, \pm 1)$, while the map with eigenvalues smaller than 1 is chosen for all other sites and frequencies

$$\text{map C} = \begin{cases} \text{map A for } n = 0, & k = \pm 1 \\ \text{map B for } n \neq 0, & k = \pm 1 \\ \text{map B for } k = 0 \\ \text{map A for } |k| \geq 2. \end{cases} \tag{20}$$

With such a design of map C, and the initial condition

$$A_{n,k}^{(j=0)} = \begin{cases} \delta \text{ for } (n, k) = (0, \pm 1) \\ 0 \text{ for all other modes,} \end{cases} \tag{21}$$

where only the unstable mode at $(n, k) = (0, \pm 1)$ is excited, we can expect to get initial growth in the direction of this unstable mode (eigenvalue larger than 1), whereas all other modes remain unexcited (eigenvalues less than 1).

Once the iteration yields local growth of the Fourier coefficients of the unstable mode, we expect that the nonlinear terms of the map, which become important for large enough $A_{n,k}^{(j)}$, will lead the iteration to a fix point corresponding to the discrete breather solution we are looking for. There is no guarantee for this to happen, since we have no knowledge about the fix point, even though we know it exists. Furthermore, we have neglected the second difference in finding the eigenvalues given by Eq. (19), from which we determine the design of map C. Thus for high amplitude solutions we cannot be sure that these eigenvalues are correct. All the design is focused on is getting the right initial growth, namely, local growth. The results show that this strategy works efficiently to give a solution.

In Fig. 3 we show the amplitude versus frequency relation for single-frequency static breather solutions to Eq. (5), centered at site $n = 0$, in the frequency domain where solutions could be found by iteration of map C. The initial excitation was chosen as $\delta = 0.1$, and 51 sites and 31 frequencies ($k_{\max} = 15$) were taken into account. Due to the rapid decay of the Fourier components in both the space and frequency domain [16] this cutoff is sufficient to ensure a solution with no measurable imperfections (energy loss, frequency deviation, etc.). This was checked by numerical integration. For both the Φ^3 and Φ^4 potentials we see that the amplitude is a decreasing function of frequency, which corresponds with earlier approximate findings [11]. We see also that the frequency domain in which solutions can be found by the Flach technique, is smaller for the Φ^3 potential than the Φ^4 potential. This seems reasonable since the nonlinear corrections to the eigenvalues for maps A and B are smallest for the Φ^4 potential. Finally we find solutions below the interval given by Eq. (11), where they should be unstable according to Eq. (10). For times $t < 5000$ we have not been able to detect any instability of these solutions numerically.

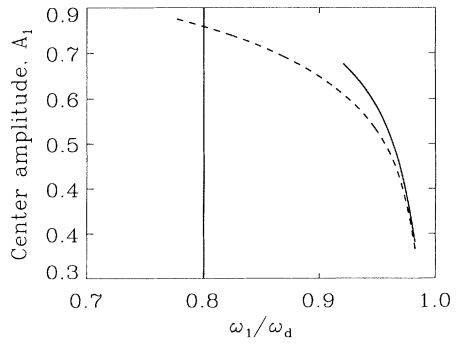

FIG. 3. Amplitude A_1 vs normalized frequency, ω_1/ω_d, for single-frequency static breather solutions to Eq. (5) found by the Flach technique, using 51 sites. The solid curve represents the Φ^3 potential $(\alpha, \beta) = (1, 0)$, and the dashed curve the Φ^4 potential $(\alpha, \beta) = (0, 1)$. The vertical line indicates the bottom of the stability band defined by Eq. (11). $\omega_d^2 = 10$, $\delta = 0.1$, and $k_{\max} = 15$.

IV. THE COLLISION PROCESS

Let us consider a typical example of a collision in the case where the amplitude of the static breather is relatively high compared with the amplitude of the moving breather. Figure 4 shows a contour plot of the energy density $\mathcal{H}_n$, defined by Eq. (4), during such a collision. It is important that the big breather is not destroyed by the collision, but remains highly localized. This means that its energy H_1 and center site n_1 can be accurately measured both before and after collision. Besides the fact that an asymmetry between the two breathers is necessary if we expect to see a difference in their behaviors in the collision, the possibility to make accurate measurements is a good reason to consider a large and a small amplitude breather, and not two small ones.

To examine the process quantitatively, we define the energy of the large breather, $H_1(t)$, as the sum of the energy density on the 11 sites centered around its center, $n_1(t)$,

$$H_1(t) \equiv \sum_{n_1(t)-5}^{n_1(t)+5} \mathcal{H}_n(t) \ , \tag{22}$$

where $n_1(t)$ is defined as the site of maximum energy in the system at time t. As the big breather is highly localized, the value of 11 sites is large enough to account for almost all its energy, and small enough to separate its energy from that of the small breather, except during a small time interval around the collision. We then define the transfer of energy from the small breather to the large one, $\Delta H_1(t)$, and the displacement of the large breather, $\Delta n_1(t)$, as

$$\Delta H_1(t) \equiv \frac{H_1(t) - H_1^0}{H_0^0} \ , \quad \Delta n_1(t) \equiv n_1(t) - n_1(0) \ . \tag{23}$$

Here H_0^0 and H_1^0 are the initial total energies of the small and big breather, respectively. With this definition $\Delta H_1 = 1$ if the big breather has consumed all the energy of the little one and $\Delta H_1 = 0$ if no energy has

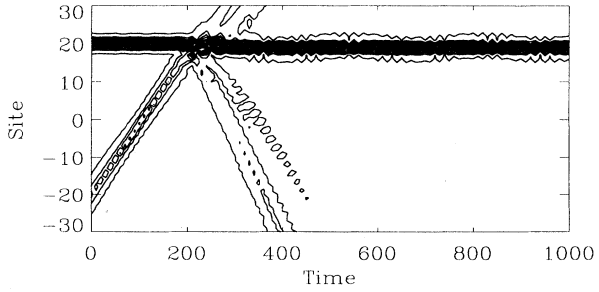

FIG. 4. Collision between a moving breather ($V_0 = 0.2$, $A_0 = 0.2$, $n_0 = -20$) and a static breather ($A_1 = 0.7$, $n_1 = 20$). Contour plot of the energy density, $\mathcal{H}_n(t)$, with 30 levels between $\mathcal{H}_n = 0.01$ and 2.16. $\omega_d^2 = 10$ and $(\alpha, \beta) = (1, 0)$ (Φ^3 potential).

been transferred. These two quantities are plotted in Fig. 5 for the collision shown in Fig. 4.

The evolution of $\Delta n_1(t)$ shows that the collision displaces the big breather by exactly 1 site, which can be understood in the following way: As the small breather approaches, the PN potential "felt" by the big breather is locally altered, such as to enable it to overcome the PN barrier. When the perturbation implied by the presence of the small breather is gone, the big breather again becomes trapped at a single site. Thus this "quantization" of the displacement is a manifestation of the lattice discreteness. The energy transfer $\Delta H_1(t = 1000) = 21\%$ is positive, indicating that the big breather has swallowed energy from the little one. However, as will become apparent from the following section, the process depends on the relative phase and energy of the two breathers. Thus we cannot conclude to energy transfer without more systematic studies. Looking at the time evolution of $\Delta H_1(t)$, it might seem that it stays constant after the collision, which would mean that a stable nonradiating breather is obtained with a higher energy than before the collision. However, as seen on the close-up, the energy of the big breather is actually decaying slowly.

Figure 6, which shows the frequency spectrum of the big breather before and after collision, explains the origin of the decay. We see that the main frequency of the breather decreases slightly from $\omega_1 = 2.897$ before the collision to $\omega_1 = 2.835$ after. This is consistent with an increase of the breather energy as indicated by Fig. 3. Moreover, the spectrum changes qualitatively. Initially the breather has only one internal frequency, but after the collision a second frequency appears close to the bottom of the phonon band. It is this frequency that leads to the radiation of energy seen in Fig. 5, through a resonance between sum frequencies and the phonon band. Although it is weak, this sum frequency, lying in the phonon band, can be seen in the figure.

This result points out that a measurement of the energy of the big breather immediately after the collision is not sufficient to draw a conclusion about energy localization, because the emerging breather has been perturbed and may lose the energy gained (if $\Delta H_1 > 0$) in the collision. However, in the simulations that we have performed, the decay rate of the perturbed breather was always very small. Thus, in a lattice where temperature fluctuations and modulational instability create a complicated pattern of phonons and small amplitude moving breathers, it seems that a big breather, once it is created, will have plenty of time to interact again with phonons or other breathers, before losing any significant amount of the energy it might have gained through a collision. All the values of ΔH_1 given henceforth have been recorded at $t = 1000$, i.e., sufficiently long after the collision to include a possible decay of the perturbed high amplitude breather.

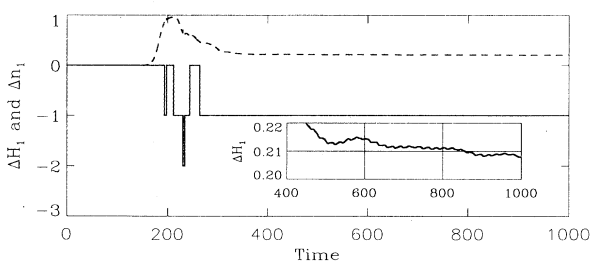

FIG. 5. Time dependence of the energy transfer ΔH_1 (dashed curve) and displacement Δn_1 (solid curve) for the collision shown in Fig. 4. The plot in the lower right corner shows a close-up of the decay of ΔH_1 after the collision.

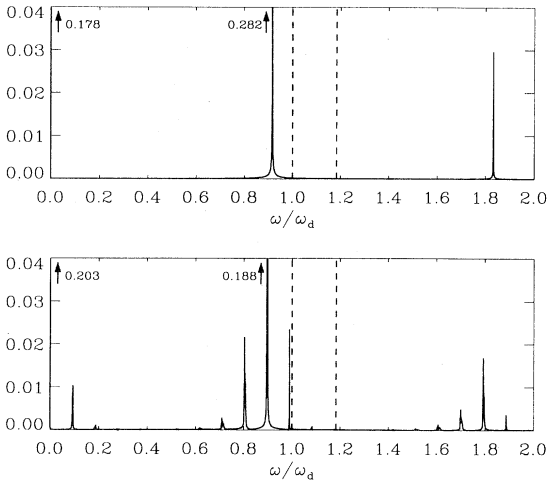

FIG. 6. Spectrum (arbitrary units) of the oscillations of the center amplitude of the static breather before and after the collision shown in Fig. 4. Top: Before the moving breather is launched ($-5000 \leq t \leq 0$). The main frequency is $\omega_1 = 2.897$. Bottom: After collision ($1000 \leq t \leq 6000$). The solution is cleaned from radiation at $t = 1000$ by setting $U_n = 0$ outside the 41 center sites. Here $\omega_1 = 2.835$. The phonon band is indicated by two dashed lines. $\omega_d^2 = 10$ and $(\alpha, \beta) = (1, 0)$ (Φ^3 potential).

V. STATISTICAL NUMERICAL CALCULATIONS

The transfer of energy from the moving breather to the static breather, ΔH_1, and the displacement of the static breather, Δn_1, during collision, depend on the relative phase and energy difference between the two breathers. We investigate this dependence statistically by simulating N collisions, in which the parameters of the small moving breather are varied randomly.

From the discussion in Sec. II, we know that the small breather is completely determined by the three parameters q_0, A_0, and V_0, where the internal wave number may be fixed at $q_0 = 0.2$ for the values of the amplitude and velocity that we consider here. Due to the setup of our numerical simulations, the initial center site, n_0, is also a determining parameter. Thus we assume a Gaussian distribution of A_0, V_0, and n_0, around the mean values $\overline{A}_0$, $\overline{V}_0$, and $\overline{n}_0$, with variations δA_0, δV_0, and δn_0. The variations have to be sufficiently small to assure a good solution.

In Fig. 7 we depict the probability distribution of ΔH_1 and Δn_1, found from $N = 200$ simulations of collisions between a static breather of amplitude $A_1 = 0.52$ at site $n_1 = 20$, and a small moving breather with random parameters A_0, V_0, and n_0. The mean values and variations are given in the figure caption. The potential is the nonsymmetric Φ^3 potential. We see that the energy transfer can be negative, but that the probability for this to occur is small (here 8 in 200). Generally ΔH_1 is positive and centered around the mean value $\overline{\Delta H_1} = 9\%$. The displacement is quantized due to the strong discreteness of the system ($\omega_d^2 = 10$) and the high amplitude of the breather. It is generally negative (195 in 200) and centered around the mean value $\overline{\Delta n_1} = -1.3$.

The random variation of the initial parameters of the small moving breather covers the whole range of relative phase differences between the breathers, but only a small interval of the relative energy difference. To explore the whole interval of energy differences we vary the amplitude A_1 of the static breather, and perform a series of 200 simulations as presented in Fig. 7 for each value of A_1. The dependence of $\overline{\Delta H_1}$ and $\overline{\Delta n_1}$ on A_1 is plotted in Fig. 8. We have depicted the results for both the Φ^3 and Φ^4 potentials to see if the symmetry of the potential is of importance. The resolution in A_1 is 0.02 and thus the fluctuations seen in the figure are actual results of the numerical calculations, and not due to lack of resolution.

From Fig. 8, we can distinguish three regions:

(i) In the limit of large A_1, the energy transfer and displacement approaches 0. Although the Flach technique does not allow as high values of A_1 for the Φ^3 potential as for the Φ^4 potential (see Sec. III and Fig. 3), the tendency is clear in both cases, especially for the displacement. An example of a collision in this regime is shown in Fig. 9. We see that the big breather acts as an almost perfect reflector (a careful investigation shows that a small amount of the energy of the small breather is still transmitted). Investigating the spectrum of the oscillations of the center amplitude of the static breather before and after collision reveals only one component, which is not noticeably affected by the collision. The probability distribution of the energy transfer shows that it is 0 on average, but that slight variations (less than 1%), both positive and negative, do occur. None of the collisions displaces the large breather, which is not surprising because it is strongly pinned by discreteness due to its large amplitude.

(ii) In the intermediate region $0.5 < A_1 < 0.7$ we see that the collision begins to affect the static breather. The energy transfer increases to about 12% for the Φ^3 potential and 16% for the Φ^4 potential, and the displacement increases to up to 2 sites.

(iii) Finally, in the low amplitude limit $A_1 < 0.5$, the energy transfer decreases. This is not surprising since we expect the energy transfer to vanish when both breathers are equivalent or when both have small amplitudes. In the former case due to symmetry and in the latter because the dynamics of the two breathers would become that of two NLS solitons that by definition does not exchange energy. Moreover, as the static breather, now rather small, is only weakly pinned by discreteness, its displacement in the collision increases and in some cases

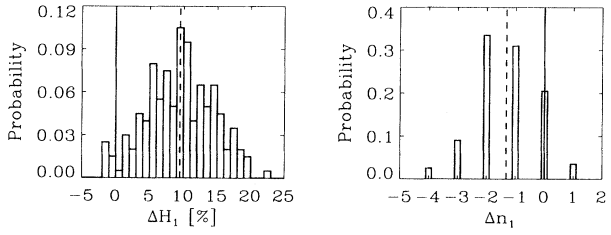

FIG. 7. Probability distribution of (left) the energy transfer $\Delta H_1(t = 1000)$ and (right) the displacement $\Delta n_1(t = 1000)$, found from $N = 200$ simulations. Dashed line indicates the mean values $\overline{\Delta H_1} = 9\%$ and $\overline{\Delta n_1} = -1.3$. The parameters of the moving breather all have a Gaussian distribution with average values $\overline{A}_0 = 0.1$, $\overline{V}_0 = 0.2$, $\overline{n}_0 = -20$ and variations $\delta A_0 = 0.05$, $\delta V_0 = 0.1$, $\delta n_0 = 10$. $A_1 = 0.52$, $n_1 = 20$, $\omega_d^2 = 10$, and $(\alpha, \beta) = (1, 0)$ (Φ^3 potential).

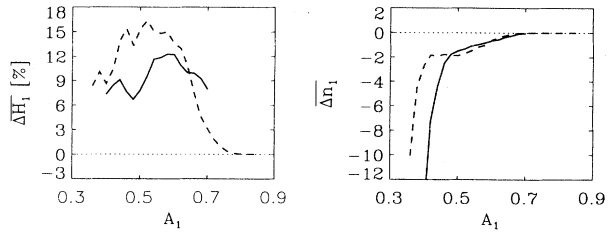

FIG. 8. Mean value of (left) the energy transfer, $\overline{\Delta H_1}(t = 1000)$ and (right) the displacement $\overline{\Delta n_1}(t = 1000)$ found from $N = 200$ simulations, as a function of A_1. The data for the moving breather are the same as in Fig. 7. $n_1 = 20$, $\omega_d^2 = 10$, and $(\alpha, \beta) = (1, 0)$ (Φ^3 potential, solid curve), $(\alpha, \beta) = (0, 1)$ (Φ^4 potential, dashed curve).

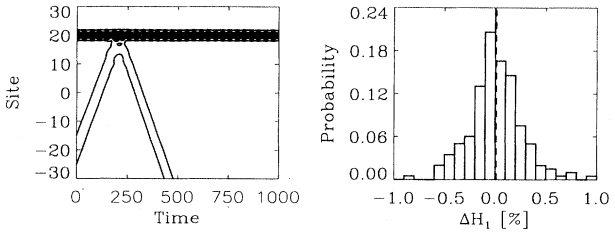

FIG. 9. Left: Collision between a moving breather ($A_0 = 0.1$, $V_0 = 0.2$, $n_0 = -21$) and a static breather ($A_1 = 0.86$, $n_1 = 20$). Contour plot of the energy density, $\mathcal{H}_n(t)$, with 30 levels between $\mathcal{H}_n = 0.02$ and 2.97. Right : Probability distribution of the energy transfer $\Delta H_1(t = 1000)$ between moving breathers and the same static breather for $N = 200$ simulations. The dashed line indicates the mean value $\overline{\Delta H_1} = 0.01\%$. The parameters of the moving breather all have a Gaussian distribution with average values $\overline{A}_0 = 0.1$, $\overline{V}_0 = 0.2$, $\overline{n}_0 = -20$ and variations $\delta A_0 = 0.05$, $\delta V_0 = 0.1$, $\delta n_0 = 10$. $\omega_d^2 = 10$ and $(\alpha, \beta) = (0, 1)$ (Φ^4 potential).

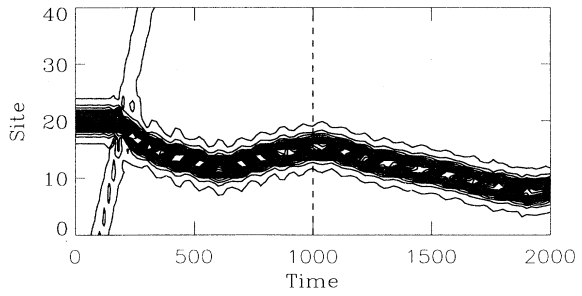

FIG. 10. Collision between a moving breather ($A_0 = 0.1$, $V_0 = 0.2$, $n_0 = -20$) and a static breather ($A_1 = 0.36$, $n_1 = 20$). Contour plot of the energy density, $\mathcal{H}_n(t)$, with 30 levels between $\mathcal{H}_n = 0.01$ and 1.18. $\omega_d^2 = 10$ and $(\alpha, \beta) = (0, 1)$ (Φ^4 potential).

the breather can start moving after the collision. A typical case is shown in Fig. 10.

It is important to notice that the investigations of a large number of breather collisions in the discrete lattice, summarized in Fig. 8, show that *on average a collision favors the growth of the larger breather*, provided that the initial energy difference is not too big, or the energy of both breathers is so small that they are in the NLS limit. Doubling the mean value and variation of the amplitude of the small breather to $(\overline{A}_0, \delta A_0) = (0.2, 0.1)$, and performing a new series of simulations, confirms this qualitative behavior.

VI. MULTIPLE COLLISIONS

The mechanism of energy transfer through collisions is physically relevant only if the small energy transfer between two low energy breathers can add up through multiple collisions and create large amplitude breathers with a reasonable lifetime. Regarding this lifetime, we have so far considered exact single-frequency solutions for the static breather, implying that such a stable state with infinite lifetime could be excited by the lattice. However, simulations have shown that, in most cases, a two-frequency solution results from a collision (see Fig. 6). We will briefly consider these points in this section and show that it indeed is possible to generate exact single-frequency breathers through multiple collisions.

To show this we look at a specific example of multiple collisions. We start out with a static single-frequency breather with amplitude $A_1 = 0.36$ (lowest possible amplitude obtainable with the Flach technique) at site $n_1 = 50$, and launch a breather of amplitude $A_0 = 0.2$ at site $n_0 = 0$, moving towards the static breather with the velocity $V_0 = 0.2$. At time $t = 1000$ we clean the solution for radiation by setting the amplitude to zero outside the 51 sites centered around the site of maximum energy and launch another small breather with the same data as the first one.

Figure 11 shows a contour plot of the energy density during such a simulation, where 20 small breathers were launched to collide with the big breather. The top and bottom panels show the result for the Φ^3 and Φ^4 potential, respectively. Initially the collisions displace the breather by a significant amount and then less and less. No clear difference between the two cases shows up, except that the dynamics with the Φ^4 potential seems to lead to less radiation and a more stable state. This is noticeable already after seven collisions. The variation of the energy of the large breather during the 20 collisions is shown in Fig. 12.

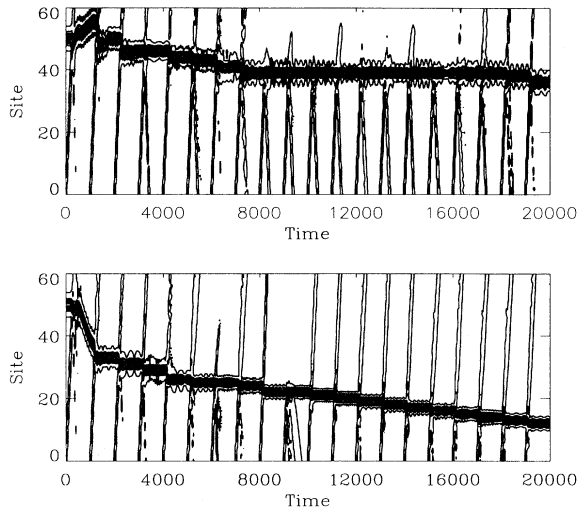

FIG. 11. Example of 20 collisions between a moving breather ($A_0 = 0.2$, $V_0 = 0.2$, $n_0 = 0$), and a static breather ($A_1 = 0.36$, $n_1 = 50$), as detailed in the text. Contour plot of the energy density, $\mathcal{H}_n(t)$ with 30 levels between $\mathcal{H}_n = 0.01$ and $\mathcal{H}_n^{\max}$. Top: $(\alpha, \beta) = (1, 0)$ (Φ^3 potential) and $\mathcal{H}_n^{\max} = 2.44$. Bottom: $(\alpha, \beta) = (0, 1)$ (Φ^4 potential) and $\mathcal{H}_n^{\max} = 3.02$. $\omega_d^2 = 10$.

Here we see more clearly that the dynamics in the case

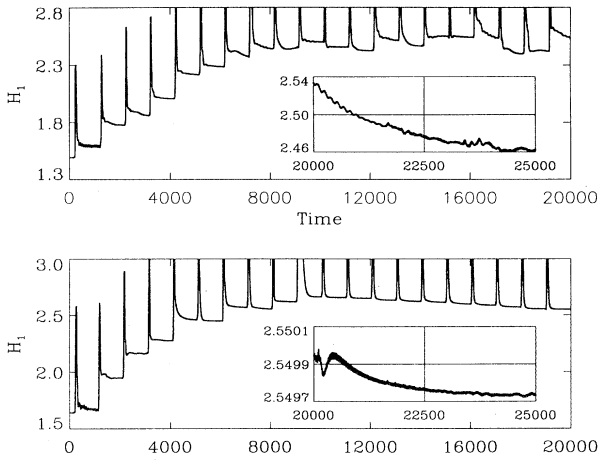

FIG. 12. Time evolution of the energy H_1 defined in Eq. (22), corresponding to Fig. 11. Each close-up shows the energy decay for $20\,000 \leq t \leq 25\,000$. The energy at $t = 20\,000$ is (top) $H_1 = 2.534$ and (bottom) $H_1(t = 20\,000) = 2.504$. Top: $(\alpha, \beta) = (1, 0)$ (Φ^3 potential). Bottom: $(\alpha, \beta) = (0, 1)$ (Φ^4 potential). $\omega_d^2 = 10$.

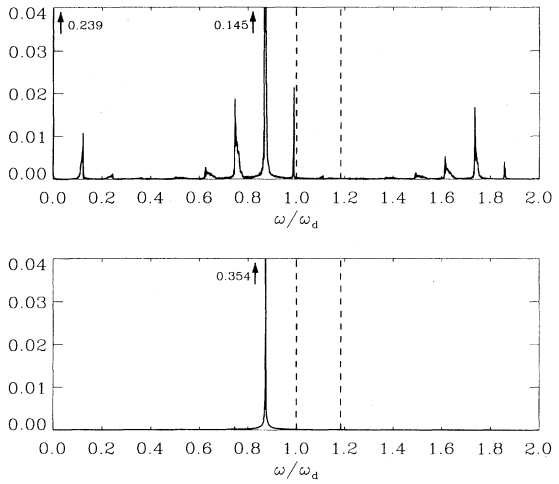

FIG. 13. Spectrum (arbitrary units) of the oscillations of the center amplitude of the static breather after the 20 collisions shown in Fig. 11. The spectrum is calculated from $20\,000 \leq t \leq 25\,000$ corresponding to the close-ups in Fig. 12. The phonon band is indicated by the two dashed lines. Top: $(\alpha, \beta) = (1, 0)$ (Φ^3 potential). The main frequency is $\omega_1 = 2.745$. Bottom: $(\alpha, \beta) = (0, 1)$ (Φ^4 potential). The main frequency is $\omega_1 = 2.760$. $\omega_d^2 = 10$.

of the symmetric Φ^4 potential is cleaner in the sense that the breather obtained after each collision radiates less energy than in the case of the nonsymmetric Φ^3 potential. After the 20 collisions a breather with an energy $H_1(t = 20\,000) = 2.534$ is obtained for the Φ^3 potential, and $H_1(t = 20\,000) = 2.550$ for the Φ^4 potential. Thus this simulation verifies that large amplitude breathers can be created by the mechanism of energy transfer. It also indicates that its amplitude saturates to a large value, and further collisions cannot increase it any more.

The physically important question is then: What is the lifetime of these breathers? The close-ups in Fig. 12 show that for the Φ^3 potential the decay is significant, while it is negligible for the Φ^4 potential. As discussed in Sec. IV this implies, respectively, a two-frequency and single-frequency solution, which is confirmed by the spectra of the two breathers shown in Fig. 13. The clean single-frequency spectrum found for the Φ^4 potential indicates that multiple collisions can really create almost exact discrete breathers in the lattice. Besides its interesting consequence for the physics of nonlinear lattices, this calculation also validates the use of single-frequency static breathers in our calculations.

VII. DISCUSSION

In this paper we have studied the exchange of energy and momentum during collision between breathers in nonlinear KG lattices. The aim has been to show that the energy exchange tends to favor the growth of the larger breather and thus represents an inherent physical mechanism to generate highly localized large amplitude excitations in nonlinear lattices. This mechanism, which was conjectured from results obtained in a particular case [12], appears to be very general. A statistical analysis based on a large number of numerical simulations has been necessary to establish it unambiguously because the results of individual collisions depend not only on the relative energies of the colliding breathers, but also on their relative phases. However, the simulations exhibit a systematic bias toward energy transfer from the smaller breather to the larger one, irrespective of the symmetry of the on-site potential (Φ^3 or Φ^4).

Our results are purely numerical. Indeed it would be interesting to get an analytical insight into the process, but up to now we failed. The reason is that this effect is intrinsically discrete and no exact solution exists, even for a single discrete breather [26]. The Flach technique that we used to find exact static breather solutions relies on numerical iteration. This method may seem like a "qualified lucky guess," but its foundation includes an important point. It is well known that localization of vibrational energy in lattices can be obtained around points of symmetry breaking, such as defects [32, 33] or kinklike distortions [33, 34]. This is exactly what this iteration scheme does; it breaks the symmetry of the translational invariant lattice at the center of the breather by choosing different maps. But the method cannot describe breather interactions. Even analytical studies of the propagation of a single discrete breather are difficult and the predictions of the pinning threshold may be off by one order of magnitude [17, 26].

In spite of the fact that we cannot yet describe the phenomenon analytically, its clear observation in the simulations is interesting because it suggests that it could exist in a large variety of discrete systems and be much more efficient than modulational instability to localize energy. One remarkable characteristic of this localization process is that it is self-regulated through different mechanisms. If a system initially is excited with an assembly of small moving breathers, then, after multiple collisions have created rather large objects, their pinning by discreteness traps them and prevents them from colliding. Moreover, even if small breathers subsist (or are excited by some energy injection mechanism), we have shown that, once they are large enough, the discrete breathers cease to absorb energy from the small ones. These regulation processes prevent a collapse of the energy into a single huge excitation, which could destroy the lattice.

The type of lattice that we have considered provides an approximate description of many physical systems from crystals to biological molecules. In numerical simulations of such thermalized lattices, we systematically found long-lived, highly localized excitations provided that discreteness and temperature were sufficiently high. This suggests that these excitations could exist in many physical systems. Such large amplitude localized modes have been observed for macromolecules like DNA [35]. The question is why. Modulational instability cannot account for such highly localized excitations. The collision mechanism discussed here provides at least a partial answer. The examples of the Φ^3 and Φ^4 models show that it appears to be rather general. Moreover, we have verified its robustness in the presence of thermal fluctuations [12]. For applications in physics, its validity in a wider range of situations remains to be demonstrated, but there are

indications that it is the case. For instance, we have here restricted our attention to harmonic interaction between sites, but recent results with a sinusoidal coupling have also exhibited examples of growth by collision although a systematic study has not yet been performed. Extending the same study to three-dimensional systems, which can also sustain localized excitations due to anharmonicity [8], would be another interesting question.

ACKNOWLEDGMENTS

We would like to thank S. Flach, T. Dauxois, C. Eilbeck, and S. Aubry for useful and stimulating discussions. S. Flach is also thanked for invaluable help. CEC is acknowledged for financial support of Contract No. SC1-CT91-0705. O.B. is now a part of the Australian National Photonics Cooperative Research Centre.

[1] R. Hobart, J. Appl. Phys. **36**, 1944 (1965).
[2] J. Krumhansl and J.R. Schrieffer, Phys. Rev. B **11**, 3535 (1975).
[3] A.R. Bishop and T.F. Lewis, J. Phys. C **12**, 3811 (1979).
[4] M. Peyrard and A.R. Bishop, Phys. Rev. Lett. **62**, 2755 (1989).
[5] A.V. Ustinov, M. Cirillo, and B.A. Malomed, Phys. Rev. B **47**, 8357 (1993).
[6] A.J. Sievers and S. Takeno, Phys. Rev. Lett. **61**, 970 (1988).
[7] A.M. Kosevich and A.S. Kovalev, Zh. Eksp. Teor. Fiz. **67**, 1793 (1974) [Sov. Phys. JETP **40**, 891 (1975)].
[8] S. Takeno, K. Kisoda, and A.J. Sievers, Prog. Theor. Phys. Suppl. **94**, 242 (1988); S.R. Bickham and A.J. Sievers, Phys. Rev. B **43**, 2339 (1991); S.R. Bickham, A.J. Sievers, and S. Takeno, *ibid.* **45**, 10 344 (1992).
[9] J.B. Page, Phys. Rev. B **41**, 7835 (1990); K.W. Sandusky, J.B. Page, and K.E. Schmidt, *ibid.* **46**, 6161 (1992).
[10] Y.S. Kivshar, Phys. Rev. E **48**, 4132 (1993).
[11] T. Dauxois, M. Peyrard, and C.R. Willis, Physica D **57**, 267 (1992); Phys. Rev. E **48**, 4768 (1993).
[12] T. Dauxois and M. Peyrard, Phys. Rev. Lett. **70**, 3935 (1993).
[13] S. Flach and C.R. Willis, Phys. Lett. A **181**, 232 (1993); S. Flach, C.R. Willis, and E. Olbrich, Phys. Rev. E **49**, 836 (1994).
[14] S. Flach and C.R. Willis, Phys. Rev. Lett. **72**, 1777 (1994).
[15] S. Flach, Phys. Rev. E **50**, 3134 (1994).
[16] S. Flach, Phys. Rev. E **51**, 3579 (1995).
[17] Ch. Claude, Yu.S. Kivshar, O. Kluth, and K.H. Spatschek, Phys. Rev. B **47**, 14 228 (1993).
[18] Y.S. Kivshar, Phys. Lett. A **173**, 172 (1993).
[19] R.S. Mackay and S. Aubry, Nonlinearity **7**, 1623 (1994).
[20] J. Rubinstein, J. Math. Phys. **11**, 258 (1970).
[21] V.M. Eleonskii, N.E. Kulagin, N.S. Novozhilova, and V.P. Silin, Teor. Mat. Fiz. **60**, 395 (1984).
[22] H. Segur and M.D. Kruskal, Phys. Rev. Lett. **58**, 747 (1987).
[23] T. Brooke Benjamin and J.E. Feir, J. Fluid Mech. **27**, 417 (1967).
[24] Y.S. Kivshar and M. Peyrard, Phys. Rev. A **46**, 3198 (1992).
[25] P. Marquié, J.M. Bilbault, and M. Remoissenet, Phys. Rev. E **51**, 6127 (1995).
[26] O. Bang and M. Peyrard, Physica D **81**, 9 (1995).
[27] J. Frenkel and T. Kontorova, J. Phys. **1**, 137 (1939); F.C. Frank and J.H. van der Merwe, Phys. R. Soc. A **198**, 205 (1949); Y. Ishimori and T. Munakata, J. Phys. Soc. Jpn. **51**, 3367 (1982); M. Peyrard and M.D. Kruskal, Physica D **14**, 88 (1984); R. Boesch and C.R. Willis, Phys. Rev. B **39**, 361 (1989).
[28] F. Nabarro, *Theory of Crystal Dislocations* (Clarendon, Oxford, 1967).
[29] D.B. Duncan, J.C. Eilbeck, H. Feddersen, and J.A.D. Wattis, Physica D **68**, 1 (1993).
[30] H. Feddersen, in *Nonlinear Coherent Structures in Physics and Biology*, edited by M. Remoissenet and M. Peyrard, Lecture Notes in Physics Vol. 393 (Springer, Berlin, 1991), p. 159.
[31] J.C. Eilbeck and R. Flesch, Phys. Lett. A **149**, 200 (1990); D.B. Duncan, J.C. Eilbeck, C.H. Walshaw, and V.E. Zakharov, *ibid.* **158**, 107 (1991); J.C. Eilbeck, in *Nonlinear Coherent Structures in Physics and Biology* (Ref. [30]), p. 143; H. Feddersen, Phys. Scr. **47**, 481 (1993).
[32] P.W. Anderson, Phys. Rev. **109**, 1492 (1958).
[33] H. Böttger, *Principles of the Theory of Lattice Dynamics* (Akademie-Verlag, Berlin, 1983).
[34] J.F. Currie, S.E. Trullinger, A.R. Bishop, and J.A. Krumhansl, Phys. Rev. B **15**, 5567 (1977).
[35] M. Gueron, M. Kochoyan, and J.L. Leroy, Nature **328**, 89 (1987); J.L. Leroy, Regards sur la biochimie **5**, 57 (1990).